ELEMENTA
Science of the Anthropocene

Dmitrenko, IA, et al. 2018. Wind-forced depth-dependent currents over the eastern Beaufort Sea continental slope: Implications for Pacific water transport. *Elem Sci Anth,* 6: 66. DOI: https://doi.org/10.1525/elementa.321

RESEARCH ARTICLE

Wind-forced depth-dependent currents over the eastern Beaufort Sea continental slope: Implications for Pacific water transport

Igor A. Dmitrenko*, Sergei A. Kirillov*, Paul G. Myers†, Alexandre Forest‡, Bruno Tremblay§, Jennifer V. Lukovich*, Yves Gratton‖, Søren Rysgaard*,¶ and David G. Barber*

Pacific water contributes significantly to the Arctic Ocean freshwater budget. Recent increases in Arctic freshwater flux, also affected by the Pacific-derived Arctic water, impact the Atlantic overturning circulation with implications for global climate. The interannual variability of the Pacific water outflow remains poorly understood, partly due to different branches of the Pacific water flow in the Arctic Ocean. The shelfbreak current over the Beaufort Sea continental slope transports ~50% of the Pacific-derived water eastward along the Beaufort Sea continental slope towards the Canadian Archipelago. The oceanographic mooring deployed over the eastern Beaufort Sea continental slope in October 2003 recorded current velocities through depths of 28–108 m until September 2005. Data analysis revealed that these highly energetic currents have two different modes of depth-dependent behaviour. The downwelling-favourable wind associated with cyclones passing north of the Beaufort Sea continental slope toward the Canadian Archipelago generates depth-intensified shelfbreak currents with along-slope northeastward flow. A surface Ekman on-shore transport and associated increase of the sea surface heights over the shelf produce a cross-slope pressure gradient that drives an along-slope northeastward barotropic flow, in the same direction as the wind. In contrast, the upwelling-favourable wind associated with deep Aleutian Low cyclones over the Alaskan Peninsula and/or Aleutian Island Arc leads to surface-intensified currents with along-slope westward flow. This northeasterly wind generates a surface Ekman transport that moves surface waters offshore. The associated cross-slope pressure gradient drives an along-slope southwestward barotropic flow. The wind-driven barotropic flow generated by upwelling and downwelling is superimposed on the background bottom-intensified shelfbreak current. For downwelling, this flow amplifies the depth-intensified background baroclinic circulation with enhanced Pacific water transport towards the Canadian Archipelago. For upwelling, the shelfbreak current is reversed, which results in surface-intensified flow in the opposite direction. These results are supported by numerical simulations.

Keywords: Upwelling; Downwelling; Depth-dependent currents; Pacific water

1. Introduction

The background shelfbreak current over the Beaufort Sea continental slope is known to be one of the most energetic features of the Beaufort Sea hydrography (e.g., Nikolopoulos et al., 2009; Dmitrenko et al., 2016; Forest et al., 2016). Along the Alaskan Beaufort Sea slope, the mean shelfbreak current flows eastward as a bottom-intensified shelfbreak jet (e.g., Nikolopoulos et al., 2009; **Figure 1a**). Over the Canadian Beaufort Sea slope, the shelfbreak current extends farther east towards the Canadian Archipelago (e.g., Forest et al., 2015, 2016; **Figure 1a**). This current plays an important role in transporting Pacific-derived water entering the Arctic Ocean via Bering Strait. Relatively fresh Pacific seawater significantly contributes to the Arctic Ocean freshwater budget and outflow. For example, the Pacific-derived Arctic water dominates the freshwater inventory over the top 150 m in western Davis Strait (Alkire et al., 2010) and comprises up to 20% of the freshwater inventory in the upper 300 m in western Fram Strait (Dodd et al., 2012). The interannual variability of the Pacific water outflow, however, is significant (e.g., Falck et al., 2005; Dodd et al., 2009).

* Centre for Earth Observation Science, University of Manitoba, Winnipeg, Manitoba, CA
† Department of Earth and Atmospheric Sciences, University of Alberta, Edmonton, Alberta, CA
‡ Laval University, Quebec, CA
§ McGill University, Montreal, Quebec, CA
‖ Institut National de la Recherche Scientifique – Eau Terre Environnement, Quebec, CA
¶ Arctic Research Centre, Aarhus University, DK
Corresponding author: Igor A. Dmitrenko (igor.dmitrenko@umanitoba.ca)

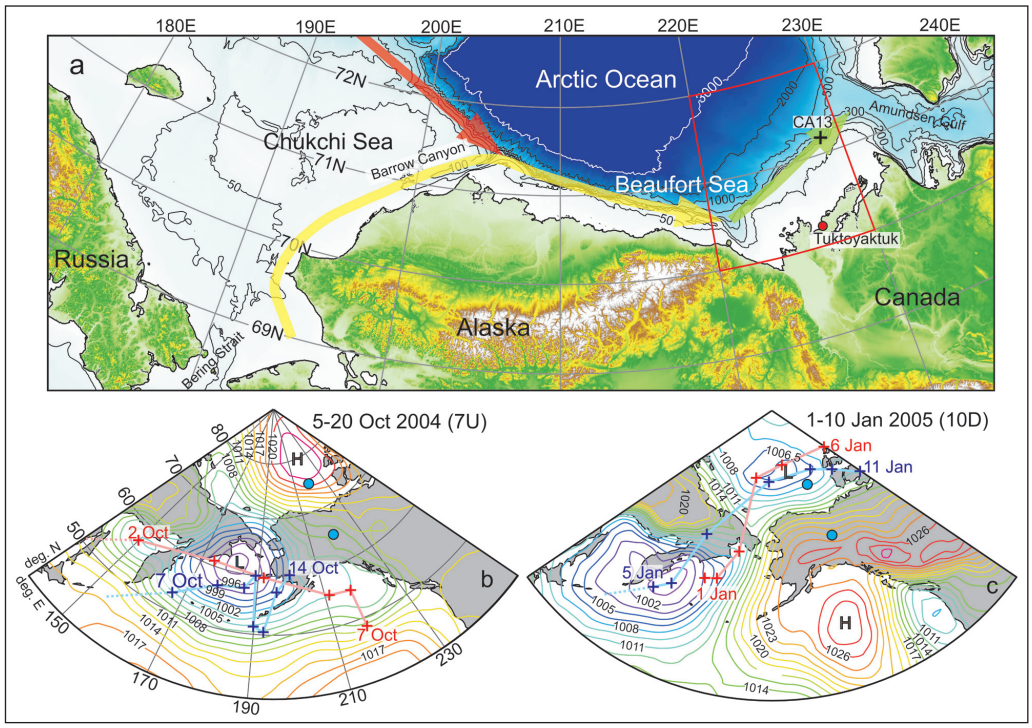

Figure 1: Maps of the Chukchi and Beaufort seas and sea level pressure. (a) Location of oceanographic mooring CA13 shown with black numbered cross. The red dot indicates the tide gauge in Tuktoyaktuk. Orange, yellow, and green arrows show circulation associated with the shelfbreak jet over the Chukchi Sea and western and eastern Beaufort Sea, respectively. The red rectangle delineates the area where the sea-ice time series is derived. **(b, c)** Mean sea level pressure (SLP, kPa) for the most energetic (b) surface-intensified velocity event during 5–20 October 2004 (#7U) and (c) depth-intensified velocity-event during 1–10 January 2005 (#10D). The SLP maps show two consecutive Pacific-born cyclones passing (b) south and (c) north of Alaska. Crosses depict the daily position of the low center for days in (b) October 2004 and (c) January 2005. The pink and light blue lines mark the cyclone pathways. Blue circles mark the grid nodes used for calculating the SLP difference. DOI: https://doi.org/10.1525/elementa.321.f1

Using numerical simulations, Winsor and Chapman (2004) revealed that without wind forcing, the Pacific Water inflow to the Chukchi Sea extends over the Beaufort shelf, with insignificant cross-shelf transport to the Canada Basin. For the wind case, Hu and Myers (2013) revealed two major pathways of Pacific Water in the Arctic Ocean, a Transpolar branch crossing the Arctic Ocean to Fram Strait and an Alaskan branch along the Beaufort Sea continental slope through the Canadian Archipelago to Baffin Bay. Those two branches advect about 70% of the Pacific Water, and half of that follows the Beaufort Sea continental slope (Hu and Myers, 2013), as confirmed by the Pacific Water tracers revealed in western Fram Strait, along northeast Greenland and Baffin Bay (e.g., Jones et al., 1998, 2003; Falck, 2001; Amon et al., 2003; Dodd et al., 2009, 2012; Alkire et al., 2010) and by numerical simulations (Watanabe, 2013; Aksenov et al., 2016). In fact, the Beaufort Sea shelfbreak current transports the Pacific-derived summer water (<100 m depth) and Pacific-derived winter water (~100–150 m depth) (e.g., Pickart, 2004; Nikolopoulos et al., 2009; von Appen and Pickart, 2012). For more details on the Pacific winter and summer water see Weingartner et al. (1998), Steele et al. (2004), and Timmermans et al. (2014). Over the Canadian Beaufort Sea slope at ~225°E, Pacific Water occupies depths down to ~130–150 m. The Pacific-derived winter water is recorded offshore over the upper continental slope at depths of ~80–160 m. The Pacific-derived summer water is more prevalent inshore occupying depths at ~50 m (Dmitrenko et al., 2016).

Recent reports on velocity observations over the eastern Beaufort Sea continental slope revealed the predominant wind-driven dynamics with the depth-dependent behaviour of currents (Barber et al., 2015; Forest et al., 2015; Dmitrenko et al., 2016). Barber et al. (2015) suggested that the appearance of early winter surface-intensified events is attributed to their generation over the Alaskan Beaufort Sea, where a delayed onset in ice cover occurs. The depth-intensified events were likely associated with along-slope northeastward transport generated by storms over the Chukchi and Alaskan Beaufort seas. In the following we present an alternative interpretation and show that the depth-dependent behaviour of currents is likely explained by local upwelling and downwelling wind forcing superimposed on the background bottom-intensified shelfbreak current. Following this interpretation, the downwelling favours depth-intensified enhanced Pacific Water transport along the Beaufort Sea continental slope with along-slope shelfbreak current towards the Canadian Archipelago and Baffin Bay. In contrast, the upwelling seems to influence, through reversals in surface-intensified flow, the Pacific Water pathway across the Arctic Ocean to Fram Strait. This potential influence is supported by numerical simulations of the Pacific water tracers.

2. Data and methods

We used velocity data from oceanographic mooring CA13 deployed over the upper Canadian Beaufort Sea continental slope at 300-m depth from 9 October 2003 to 4 September 2005 at 71°21.356'N, 228°38.176'E (**Figure 1a**). The mooring description can be found in Dmitrenko et al. (2016). For this study, we used only velocity records from the 300 kHz upward-looking Workhorse Sentinel acoustic Doppler current profilers (ADCPs) by Teledyne RD Instruments at 119-m depth. The velocity data was obtained at 8-m depth intervals, with a 1-h ensemble time interval and 30 pings per ensemble. The first bin was located at 10 m above the transducer. The RDI ADCP precision and resolution are ± 0.5% and ± 0.1 cm s^{-1}, respectively. The standard deviation for an ensemble average of 30 pings for the 8-m depth cell size is reported by RDI to be 1.19 cm s^{-1}. The compass accuracy is ±2°. The magnetic deviation was added. The along-slope direction was determined to be 64°T using the scatterplot of the daily mean velocity data following Dmitrenko et al. (2016). Examples of these scatterplots for depths of 28 m and 108 m are shown in **Figure 2**.

The sea level atmospheric pressure (SLP) was obtained from the National Centers for Environmental Prediction (NCEP) (Kalnay et al., 1996). The horizontal resolution of the NCEP-derived data is 2.5° latitude. We used the SLP difference along the 220°E meridian from 65°N to 75°N (**Figure 1b** and **c**) as a descriptor of atmospheric circulation for further comparison with the velocity time series. Negative and positive SLP differences correspond to cyclones passing south and north of the Beaufort Sea coast, respectively (**Figure 1b** and **c**). Sea-ice concentrations are derived from the Advanced Microwave Scanning Radiometer for EOS-AMSR-E with errors less than 10% for concentrations above 65% (Spreen et al., 2008). The spatial grid resolution for ice concentration is 6.25 km. The time series of sea-ice concentration was obtained by averaging the daily data at all grid nodes over the eastern Beaufort Sea area limited by 220°E to 230°E and 70°N to 72°N. For sea surface height (SSH) records, we used the hourly tide gauge data from Tuktoyaktuk (**Figure 1a**).

Following Barber et al. (2015), we used the kinetic energy, $E = (U^2 + V^2)/2$, derived from the zonal (U) and meridional (V) components of the current velocity to identify the major energetic events exceeding the two standard deviation threshold of ~500 cm^2 s^{-2}. The kinetic energy of currents over the eastern Beaufort Sea continental slope is mainly affected by the along-slope current component (Kulikov et al., 1998; Williams et al., 2006; Dmitrenko et al., 2016). For CA13, the maximum variability of currents is also consistent with along-slope direction (**Figure 2**), explaining ~70% of the total velocity variability. Thus, major energetic events are mainly associated with along-slope flow dynamics.

Overall, we identified thirteen major energetic events (**Figure 3**). Among them, four events are clearly attributed to the depth-intensified flow (#3, 4, 6 and 10D; pink shading in **Figure 3**). Six events are associated with the surface-intensified or barotropic flow (#1, 2, 7, 8, 9, and 12U; blue shading in **Figure 3**). While events #5U and 11U are depth-intensified, we have highlighted them with blue shading. In the following we show that these two events are consistent with upwelling-favourable atmospheric forcing that usually drives the surface-intensified events. Vice versa, event #13D is surface-intensified, but it is highlighted with pink shading because it is consistent with downwelling-favourable atmospheric forcing.

The passive tracer analysis was carried out in a simulation of the Nucleus for European Modeling of the Ocean (NEMO) version 3.4 (Madec, 2008). The Arctic and the Northern Hemisphere Atlantic configuration, run at 1/12 degree, was used. The horizontal resolution over the western Arctic is ~4–5 km. This distance is about two-three times less compared to estimates of the first baroclinic

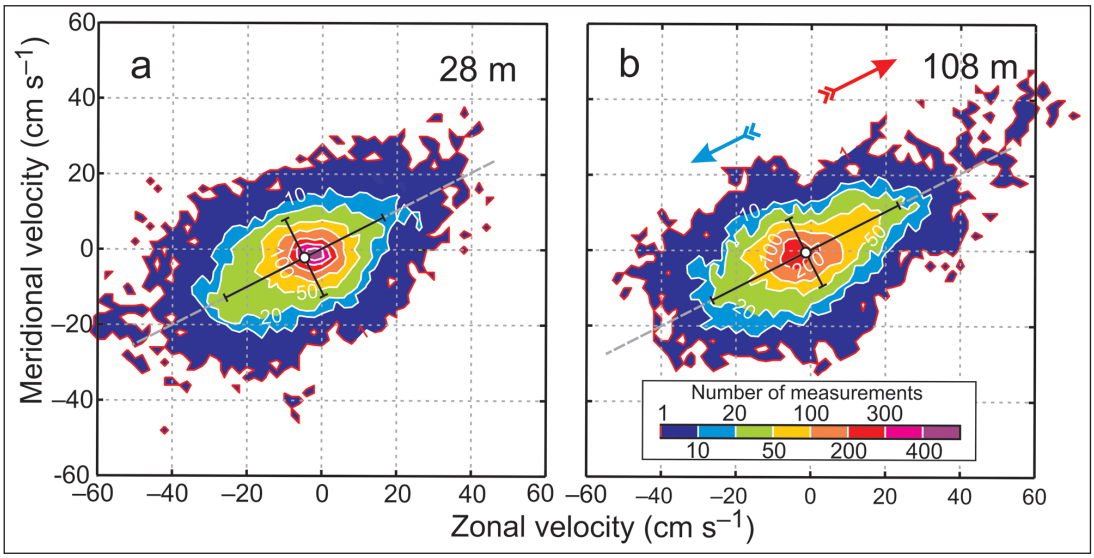

Figure 2: Scatterplots of the 24-h mean velocity at two depths. Velocity measured at depths of **(a)** 28 m and **(b)** 108 m. Gray dashed lines show the least squares regression associated with along-slope direction to 64°T. White barred dots depict the mean ± two standard deviations. Blue and red arrows indicate upwelling- and downwelling-favourable wind, respectively. DOI: https://doi.org/10.1525/elementa.321.f2

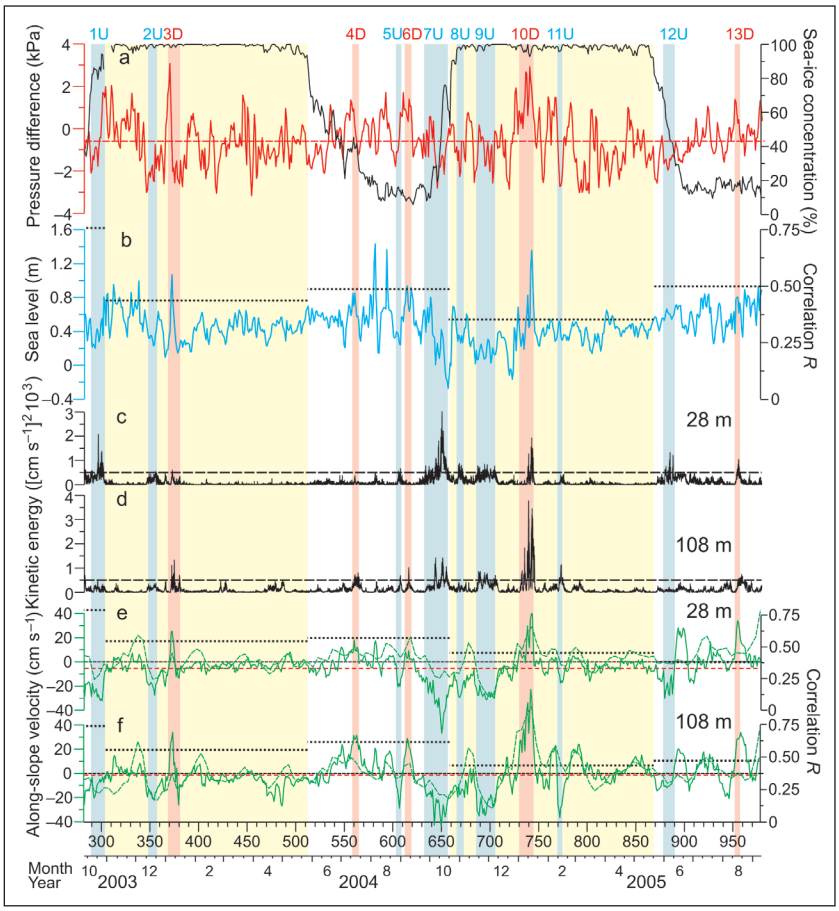

Figure 3: Time series data at the mooring location and in Tuktoyaktuk. (a) Daily mean SLP difference across the Beaufort Sea coast (kPa, red) and sea-ice concentration over the eastern Beaufort Sea (%, black); **(b)** SSH (m, blue) in Tuktoyaktuk; current kinetic energy for water depths of **(c)** 28 m and **(d)** 108 m ($cm^2\ s^{-2}$, black); and measured (solid green) and simulated (dashed green) along-slope (positive northeastward) velocity for depths of **(e)** 28 m and **(f)** 108 m ($cm\ s^{-1}$). All energetic events exceeding the two standard deviation threshold (depicted in c and d by horizontal dashed lines) are highlighted with red and blue shading for the depth-intensified (downwelling, D) and surface-intensified (upwelling, U) events, respectively, with their reference numbers on the top. Yellow shading highlights occurrence of sea-ice cover with concentration exceeding 90%. Horizontal dotted lines show correlations (R) between SLP difference and (b) SSH and (e and f) along-slope velocities for different ice conditions. (a, e and f) Red dashed lines depict 2-year means. DOI: https://doi.org/10.1525/elementa.321.f3

Rossby radius of deformation over the Beaufort Sea continental slope (~6–12 km; Nurser and Bacon, 2014), which suggests that the model permits eddies and boundary current instabilities. The sea-ice module used here is the Louvain la-Neuve Ice Model Version 2 with an elastic-viscous-plastic rheology (Hunke and Dukowicz, 1997), including both thermodynamic and dynamic components (Fichefet and Maqueda, 1997). The model domain covers the Arctic and the Northern Hemisphere Atlantic with two open boundaries, one close to Bering Strait in the Pacific Ocean and the other one at 20°S across the Atlantic Ocean. Open boundary conditions (temperature, salinity and horizontal ocean velocities) are derived from the monthly Global Ocean Reanalysis and Simulations produced by Mercator Ocean (Masina et al., 2017). The simulation was integrated from 1 January 2002 to 31 December 2016, driven with atmospheric forcing data of high temporal (hourly) and spatial resolution (33 km) provided by the Canadian Meteorological Centre Global Deterministic Prediction System ReForecasts dataset (Smith et al., 2014). There is no salinity restoring.

Further details, as well as model evaluation, can be found in Hu et al. (2018) and Courtois et al. (2017). In particular, the model is capable of realistically reproducing water dynamics over the eastern Beaufort Sea continental slope (**Figure 3e** and **f**). Passive tracer is introduced into the model at Bering Strait (which is close to one of the open boundaries of the model), starting from the beginning of the experiment on 1 January 2002. The amount of tracer input is proportional to the flux in each grid cell at Bering Strait. Thus the tracer flux replicated the seasonal and inter-annual variability of the Bering Strait inflow. Fields are presented as depth-integrated layer thickness.

3. Results

The SLP difference across the eastern Beaufort Sea continental slope is conditioned by the low-pressure systems passing south and north of the Beaufort Sea coast (**Figures 1b, 1c** and **3a**). A negative SLP difference corresponds to the southward cyclonic pathway and upwelling-favourable northeasterly wind (e.g., 5–20 October 2004; **Figure 1b**), while a positive difference is associated

with northward cyclonic pathway and the downwelling-favourable southwesterly wind (e.g., 1–10 January 2005; **Figure 1c**). The 2-year mean negative SLP difference (–0.6 kPa; red dashed line in **Figure 3a**) corresponds to the climate-mean large-scale atmospheric circulation controlled by the Beaufort High to the north and the Aleutian Low to the south (e.g., Kirillov et al., 2016). The sea-ice concentration time series shows that from October to May the southern part of the Beaufort Sea is sea-ice covered (**Figure 3a**). The consolidated ice cover partly isolates the water column from the wind stress affecting SSH and water dynamics, as we discuss below.

SSH shows synoptic scale variability that can be attributed partly to wind forcing. The SLP difference correlates positively to SSH with correlation coefficient r = 0.41 (**Figure 3b**; hereafter all correlations are statistically significant with 95% confidence). This result is consistent with a surface Ekman on-shore and off-shore transport in response to the along-shore winds associated with cyclonic activity.

A 2-year velocity time series from the eastern Beaufort Sea continental slope shows the mean southwestward (~240°) surface-intensified flow decreasing from ~5 cm s^{-1} at 28 m to 1 cm s^{-1} at 108-m depth (**Figures 2, 3e** and **f**). Velocity data also reveal the depth-dependent behaviour of currents, with events identified according to a gradual decrease or increase of their kinetic energy (**Figure 3c** and **d**) and along-slope velocity (**Figure 3e** and **f**) with depth. The surface-intensified events show the southwestward along-slope flow with daily mean velocity decreasing from ~60 cm s^{-1} at 28-m to 40 cm s^{-1} at 108-m depth for the major surface-intensified event #7U (**Figure 3e** and **f**). The associated kinetic energy decreased by more than half (**Figure 3c** and **d**). In contrast, the depth-intensified events demonstrate the northeastward along-slope flow with velocity increasing from 50 cm s^{-1} at 28 m to 70 cm s^{-1} at 108-m depth for the major depth-intensified event #10D (**Figure 3e** and **f**). This increase is associated with a doubling in the current kinetic energy (**Figure 3c** and **d**).

The water dynamics along the eastern Beaufort Sea continental slope are found to be consistent with wind forcing. The time series of current kinetic energy (**Figure 3c** and **d**) was compared to the SLP difference (**Figure 3a**) and to SSH (**Figure 3b**). The occurrence of the major depth-intensified events corresponds to the SLP low over the Beaufort Sea and to the SSH elevated over the coast (except surface-intensified events #5U and #11U). In contrast, the major surface-intensified events are associated with a negative anomaly of the SLP difference and SSH over the coast (except event #13D). For the depth-intensified events, the SLP low over the Beaufort Sea is conditioned by the Pacific-born cyclones migrated from the northeast Pacific Ocean to the Chukchi Sea and further eastward towards the Canadian Archipelago, as was observed for the major depth-intensified event #10D during 1–10 January 2005 (**Figure 1c**). For the surface-intensified events, a reversal of the SLP difference is conditioned by deep Aleutian Low cyclones near the Alaskan Peninsula and/or Aleutian Island Arc, as we revealed for the major surface-intensified event #7U during 5–20 October 2004 (**Figure 1b**). The along-slope velocity lagged the SLP gradient by 3 days with correlations from 0.42 at 28 m to 0.47 at 108-m depth (**Figure 3e** and **f**). These results indicate that the along-slope northeastward current consistently occurred following the SLP positive difference and associated westerly winds. In contrast, the along-slope current is consistently reversed following easterly winds associated with a negative SLP difference (**Figure 3a, 3e** and **3f**). A 3-day lag is consistent with that for the maximal onshore salt flux across the shelf break, which occurred in ~3 days after the onset of the upwelling-favourable wind conditions (Carmack and Chapman, 2003).

The ice cover over the eastern Beaufort Sea slightly reduced the relationship of the atmospheric forcing to the sea-level and water dynamics. Once the consolidated pack ice (with concentrations exceeding 90%) has formed in the middle/end of October 2004/2003, the correlations of the SLP difference to SSH and along-slope current become less. In contrast, during the ice-free summers the correlation is higher, with an exception for the 28-m depth velocity record during summer 2005 (**Figure 3**). Moreover, from January/February 2004/2005 when the first-year ice pack has become ~1–2 m thick until the rapid retreat of sea ice in June, the SLP time series data clearly correlate to the SSH and currents but there is a discrepancy in the amplitude of the signals. During this period no major current events were observed (**Figure 3c** and **d**). Unfortunately, sea-ice thickness data are not available for this analysis.

Overall, all major current events highlighted in **Figure 3** are associated with cyclones over the Beaufort Sea (positive SLP difference in **Figure 3a**, pink shading) or the cyclones near the Alaskan Peninsula or Aleutian Island Arc (negative SLP difference in **Figure 3a**, blue shading). However, there are several exceptions to the depth-dependent regularities described above. The depth-intensified events #5U and #11U are associated with negative SLP difference and SSH anomalies. They also show the southwestward flow that is consistent with ocean response to the atmospheric forcing of the surface-intensified events #1, 2, 7–9, and 12U (**Figure 3**). In contrast, the surface-intensified event #13D shows positive SLP difference and SSH anomalies as well as northeastward flow. These features are consistent with ocean response to the atmospheric forcing for depth-intensified events #3, 4, 6 and 10D (**Figure 3**).

4. Discussion and conclusions

We suggest that the depth-dependent behaviour of along-slope currents is in line with patterns of atmospheric forcing schematically shown in **Figure 4a** and **b**. The atmospheric forcing for the major surface-intensified events is suggested to be upwelling-favourable. The ocean response to this atmospheric forcing is consistent with ocean upwelling (U events in **Figure 3**). The cyclones passing near the Alaskan Peninsula and eastern Aleutian Island Arc (negative SLP difference; **Figures 1b**, **3a** and **4a**) generate easterly upwelling-favourable winds with a surface Ekman transport that moves surface waters offshore. The associated cross-slope pressure gradient drives an along-slope southwestward barotropic flow as described by Pickart et al. (2009, 2013) and Schulze and Pickart (2012), elucidating the role of sea-ice conditions in upwelling phenomena in the western Beaufort Sea.

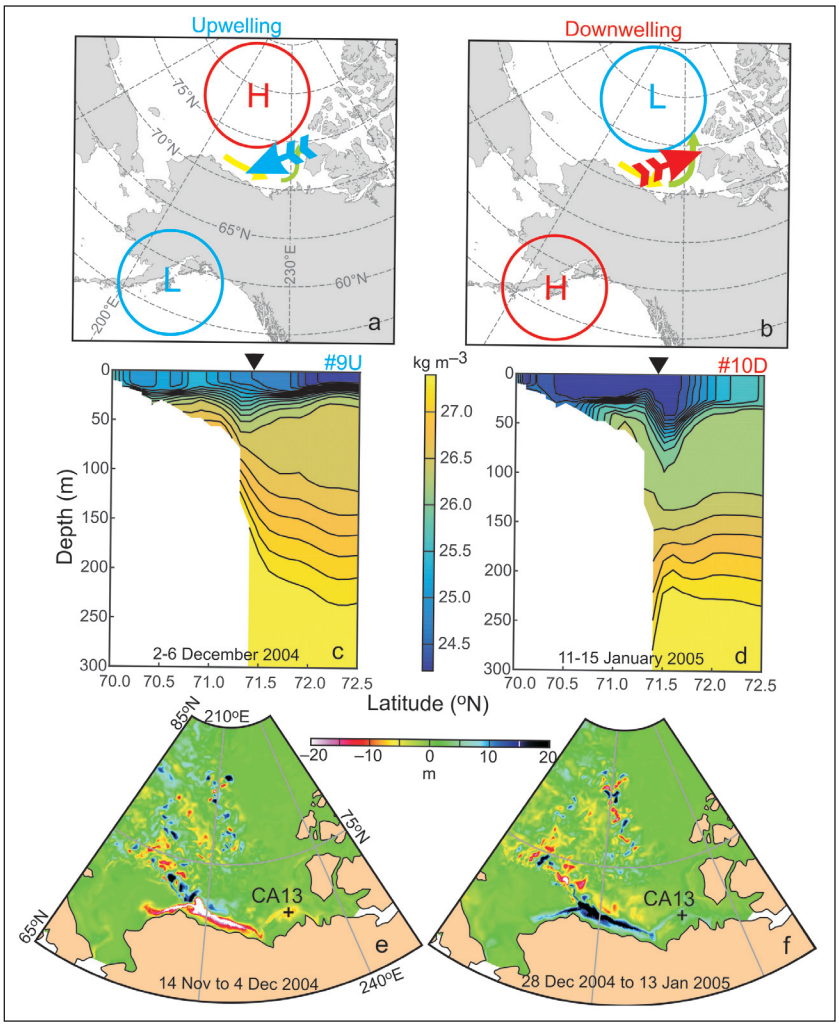

Figure 4: (a, b) Atmospheric forcing and (c–f) simulated water response. Schematic depiction showing atmospheric forcing for **(a)** upwelling and **(b)** downwelling along the eastern Beaufort Sea continental slope. Blue and red arrows indicate geostrophic wind associated with concurrence between atmospheric low and high depicted by blue and red circles, respectively. Yellow and green arrows show circulation with shelfbreak jet over the western and eastern Beaufort Sea, respectively, intensified by local downwelling. **(c, d)** Simulated cross-slope density distribution at 229°E for the end of (c) upwelling #9U and (d) downwelling #10D. Triangles on the top identify mooring position. **(e, f)** Difference in Pacific water tracers (m) from beginning to end of (e) upwelling #9U and (f) downwelling #10D highlights (e) westward and (f) eastward Pacific water transport. DOI: https://doi.org/10.1525/elementa.321.f4

In contrast, the atmospheric forcing for the major depth-intensified events is downwelling-favourable, and the ocean response to this forcing is consistent with ocean downwelling (D events in **Figure 3**). The cyclones passing north of the Beaufort Sea continental slope toward the Canadian Archipelago (positive SLP difference; **Figures 1c, 3a** and **4b**) generate the downwelling-favourable westerly winds. A surface Ekman on-shore transport and associated storm surge over the coast (**Figure 3b**) produce a cross-slope pressure gradient that drives an along-slope northeastward geostrophic flow (**Figure 3f** and **e**), in the same direction as the wind as described for the eastern Beaufort Sea by Dmitrenko et al. (2016).

Our results show the role of sea ice in transmitting wind stress to the water column. Correlations (**Figure 3b**, **e** and **f**) show that in general the response of water and sea-level dynamics to wind forcing is strongest during the open-water season and weakest for the ice-covered season. However, during the fall in the partial ice-covered season with sea-ice concentrations ranging from 50% to 100% (12 October–1 November 2003 and 11–31 October 2004; **Figure 3a**) the correlation at 128-m depth increased to 0.75 and 0.63 for 2003 and 2004, respectively. At 28-m depth the correlation was 0.57 and 0.4, respectively. These results are consistent with those of Schulze and Pickart (2012). Using velocity data from a mooring array deployed from August 2002 to September 2004 over the western Beaufort Sea continental slope, they revealed that water column response to wind forcing is strongest for the partial ice-cover conditions due to the ability of freely moving ice keels to transmit wind stress through the pack ice. In contrast, during the spring period of 2004 and 2005 this effect was not pronounced, likely because of the difference in mobility for the newly formed and one-year-old pack ice.

The suggested scenario of the water column response to wind forcing is fully consistent with that described by Watanabe (2013) based on numerical simulations. The zone of Ekman convergence (downwelling) occurs over the Beaufort Sea continental slope in response to low SLP in the Canada Basin intensifying the eastward

shelfbreak current. In contrast, the zone of Ekman divergence (upwelling) is observed when the Beaufort High prevails, reversing the eastward shelfbreak current.

What is the reason for the different depth-dependent behaviour for the upwelling and downwelling events? For the western Beaufort Sea continental slope Pickart (2004), Nikolopoulos et al. (2009), von Appen and Pickart (2012) and Lin et al. (2016) reported an along-slope baroclinic flow, which is consistent with the eastward shelfbreak current. Based on analysis of energetics, von Appen and Pickart (2012) speculated that only the depth-intensified mode of this current is able to flow as far as the Canadian Beaufort Sea and Canadian Arctic Archipelago For the Canadian (eastern) Beaufort Sea continental slope, Dmitrenko et al. (2016) also suggested the depth-intensified shelfbreak flow based on an interpretation of the long-term mean cross-slope summer salinity distribution. For the downwelling storm in January 2005 (event #10D), Dmitrenko et al. (2016) proposed that the wind-forced along-slope barotropic flow superimposed on the background depth-intensified shelfbreak current enhances the along-slope northeastward transport. Following Dmitrenko et al. (2016) and neglecting non-linear interactions, we speculate that the wind-driven barotropic flow generated by upwelling and downwelling wind forcing is superimposed on the background bottom-intensified shelfbreak current. For the downwelling storms, this effect amplifies the depth-intensified background circulation with enhanced Pacific water transport towards the Canadian Archipelago. For the upwelling storms, the shelfbreak current is reversed, which results in surface-intensified flow in the opposite direction. In this case, the Pacific water eastward transport along the Beaufort Sea continental slope shuts down. This suggestion is in line with results of the long-term (2002–2011) observations of the Pacific water boundary current over the western Beaufort Sea continental slope reported by Brugler et al. (2014).

Our interpretation is also consistent with results of the Pacific water tracer simulations (**Figure 4c–f**). The tracer response to the consecutive upwelling and downwelling events 9U and 10D differs between them. Downwelling over the eastern Beaufort Sea continental slope (event #10D; **Figure 4d**) favours the eastward Pacific water transport along the Beaufort Sea continental slope toward the Canadian Archipelago (blue color in **Figure 4f**). In contrast, upwelling (event #9U; **Figure 4c**) blocks the background geostrophic northeastward flow. This blockage results in the Pacific water retreat from the southern Beaufort Sea (red color in **Figure 4e**), promoting its transport across the Arctic Ocean to Fram Strait.

The existence of a mean bottom-intensified shelfbreak current in the western Beaufort Sea is commonly accepted (e.g., Pickart, 2004; Nikolopoulos et al., 2009; von Appen and Pickart, 2012). For the eastern Beaufort Sea, Dmitrenko et al. (2016) showed that the summer-mean cross-slope salinity and density distributions are consistent with the bottom-intensified northeastward shelfbreak current. The isohalines and isopycnals adjacent to the upper slope are sloping upward near the outer shelf and upper slope, while in the deeper layer they slope downward. The background bottom-intensified northeastward flow, however, is not obvious from our velocity data. We speculate that our measurements do not show the thermohaline-driven depth-intensified northeastward flow because this signal is likely masked by the wind-driven water dynamics. The SLP difference in **Figure 3a** shows the negative mean that corresponds to climatic predominance of the Beaufort High, especially during the fall and winter months (e.g., Asplin et al., 2009; Kirillov et al., 2016), which is also consistent with results by Yang (2009). He reported on the seasonal tendency in the SLP gradient between the Beaufort High and Aleutian Low, which is enhanced in late fall and winter due to deepening of the Aleutian Low. This tendency is also in line with

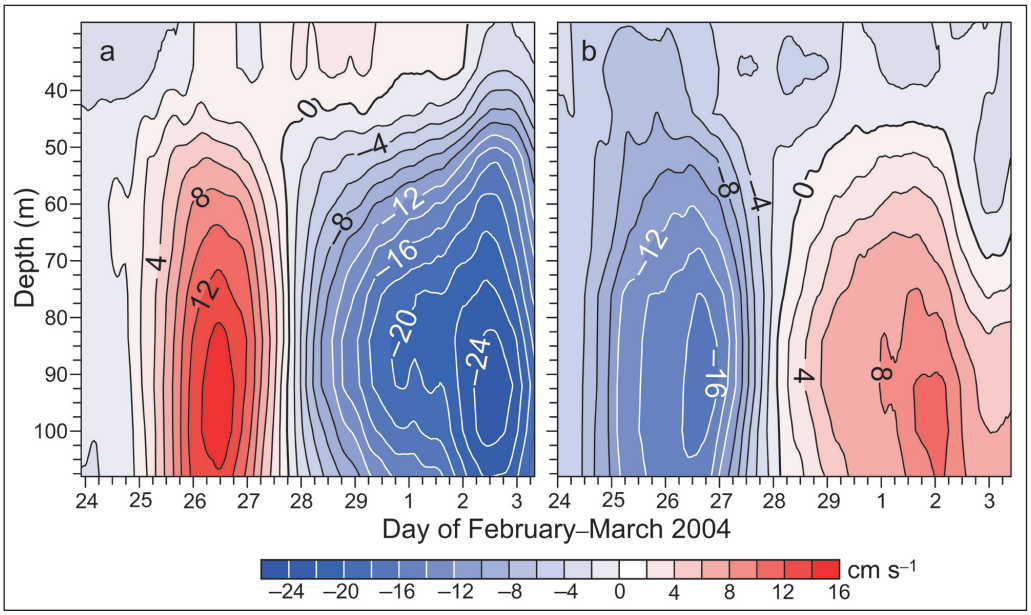

Figure 5: An enlarged view of the February–March 2004 event #11U. (a) Zonal and **(b)** meridional current (cm s^{-1}) records as a function of depth (m); ADCP records from 24 February to 3 March 2004. DOI: https://doi.org/10.1525/elementa.321.f5

seasonal occurrence of cyclonic atmospheric circulation over the Beaufort Sea reported by Asplin et al. (2009) as also evident from **Figure 3a**.

Results suggest that the sea ice also plays a role for generating major upwelling and downwelling events. During fall, the pack ice amplifies the wind stress through enhanced drag (e.g., Williams et al., 2006; Schulze and Pickart, 2012; Martin et al., 2014). This effect can be the case for events #2U, 3D, 8U, 9U, 10D (**Figure 3**). During February–May when the first-year ice pack becomes ~1–2 m thick (not shown), it significantly reduces the wind stress from the water column, and no major upwelling and downwelling events have been recorded (**Figure 3**).

Exceptions to the depth-dependent behaviour found for the upwelling events #5U and 11U and downwelling event #13D are not obvious. They may be associated with additional thermohaline forcing in response to summer freshwater flux (#13D). Moreover, the velocity time series shows rotary currents consistent with meandering of the shelfbreak current (#5U and 13D) or suggestive of an eddy passed by the mooring (#11U; **Figure 5**). Note that eddies are ubiquitous over the Arctic Ocean continental slope (e.g., Dmitrenko et al., 2008), and particularly over the Beaufort Sea continental slope (e.g., Spall et al., 2007; O'Brien et al., 2011). The eddy carrying entrained suspended particles was identified on the ADCP velocity (**Figure 5**) and acoustic backscatter (not shown) time series for 25 February–3 March 2005. Finally, none of the three exceptional events was reproduced by atmospheric-driven simulations (**Figure 3e** and **f**), suggesting that they are of different origin.

Following our results, the downwelling-favourable wind is suggested to drive an enhanced Pacific Water shelfbreak current toward the Canadian Archipelago. Thus, recurring downwelling favours the Pacific Water transport with an Alaskan route to Baffin Bay. For recurring upwelling, the eastward-flowing Pacific Water shelfbreak jet is expected to reverse, which likely favours the Pacific Water transport with a Transpolar route across the Arctic Ocean to Fram Strait. We note that our oversimplified approach is insufficient for prescribing the entire variety of the Pacific Water pathways in the Arctic Ocean and their external drivers. The deficiency of our analysis, particularly the lack of quantitative estimates of the Pacific Water transport for the upwellings and downwellings, clearly defines a necessity for numerical simulations using idealised recurring upwelling and downwelling atmospheric forcing to further our understanding of the Pacific Water transport in the Arctic Ocean.

Data Accessibility Statement

The velocity data are available through the Polar Data Catalogue at https://www.polardata.ca/pdcsearch/, CCIN Reference #11653 (Gratton et al., unpublished).

Acknowledgements

The model experiments were performed on Compute Canada infrastructure. This work is a contribution to the Arctic Science Partnership and ArcticNet.

Funding information

This study was funded by the CERC and CRC programs and NSERC (grants RGPIN 03606 to IAD, and RGPIN 04357 and RGPCC 433898 to PGM).

Competing interests

The authors have no competing interests to declare.

Author contributions

- Contributed to conception and design: ID, SK, JL, AF
- Contributed to acquisition of data: YG, AF
- Contributed to analysis and interpretation of data: ID, SK, PM, JL, BT, SR, DB
- Drafted and/or revised the article: ID, PM, JL, BT, SR
- Approved the submitted version: ID

References

Aksenov, Y, Aksenov, Y, Karcher, M, Proshutinsky, A, Gerdes, R, de Cuevas, B, Golubeva, E, Kauker, F, Nguyen, AT, Platov, GA, Wadley, M, Watanabe, E, Coward, AC and **Nurser, AJG.** 2016. Arctic pathways of Pacific Water: Arctic Ocean Model Intercomparison experiments. *J Geophys Res Oceans* **121**: 27–59. DOI: https://doi.org/10.1002/2015JC011299

Alkire, MB, Falkner, KK, Boyd, T and **Macdonald, RW.** 2010. Sea-ice melt and meteoric water distributions in Baffin Bay and the Canadian Arctic archipelago. *J Mar Res* **68**(6): 767–798. DOI: https://doi.org/10.1357/002224010796673867

Amon, RMW, Budeus, G and **Meon, B.** 2003. Dissolved organic carbon distribution and origin in the Nordic Seas: Exchanges with the Arctic Ocean and the North Atlantic. *J Geophys Res* **108**(C7): 3221. DOI: https://doi.org/10.1029/2002JC001594

Asplin, MG, Lukovich, JV and **Barber, DG.** 2009. Atmospheric forcing of the Beaufort Sea Ice Gyre: Surface pressure climatology and sea ice motion. *J Geophys Res* **114**(C00A): 06. DOI: https://doi.org/10.1029/2008JC005127

Barber, DG, Hop, H, Mundy, CJ, Else, B, Dmitrenko, IA, Tremblay, J-E, Ehn, JK, Assmy, P, Daase, M, Candlish, LM and **Rysgaard, S.** 2015. Selected physical, biological and biogeochemical implications of a rapidly changing Arctic Marginal Ice Zone. *Prog Oceanogr* **139**: 122–150. DOI: https://doi.org/10.1016/j.pocean.2015.09.003

Brugler, ET, Pickart, RS, Moore, GWK, Roberts, S, Weingartner, TJ and **Statscewich, H.** 2014. Seasonal to interannual variability of the Pacific water boundary current in the Beaufort Sea. *Progr Oceanogr* **127**: 1–20. DOI: https://doi.org/10.1016/j.pocean.2014.05.002

Carmack, E and **Chapman, DC.** 2003. Wind-driven shelf/basin exchange on an Arctic shelf: The joint roles of ice cover extent and shelfbreak bathymetry. *Geophys Res Lett* **30**: 1778. DOI: https://doi.org/10.1029/2003GL017526

Courtois, P, Hu, X, Pennelly, C, Spence, P and **Myers, PG.** 2017. Mixed layer depth calculation in deep convection regions in ocean numerical models.

Ocean Modelling **120**: 60–78. DOI: https://doi.org/10.1016/j.ocemod.2017.10.007

Dmitrenko, IA, Kirillov, SA, Forest, A, Gratton, Y, Volkov, DL, Williams, WJ, Lukovich, JV, Belanger, C and **Barber, DG.** 2016. Shelfbreak current over the Canadian Beaufort Sea continental slope: Wind-driven events in January 2005. *J Geophys Res Oceans* **121**. DOI: https://doi.org/10.1002/2015JC011514

Dmitrenko, IA, Kirillov, SA, Ivanov, VV and **Woodgate, RA.** 2008. Mesoscale Atlantic water eddy off the Laptev Sea continental slope carries the signature of upstream interaction. *J Geophys Res* **113**(C07): 005. DOI: https://doi.org/10.1029/2007JC004491

Dodd, PA, Heywood, KJ, Meredith, MP, Naveira-Garabato, AC, Marca, AD and **Falkner, KK.** 2009. Sources and fate of freshwater exported in the East Greenland Current. *Geophys Res Lett* **36**(L19): 608. DOI: https://doi.org/10.1029/2009GL039663

Dodd, PA, Rabe, B, Hansen, E, Falck, E, Mackensen, A, Rohling, E, Stedmon, C and **Kristiansen, S.** 2012. The freshwater composition of the Fram Strait outflow derived from a decade of tracer measurements. *J Geophys Res* **117**(C11): 005. DOI: https://doi.org/10.1029/2012JC008011

Falck, E. 2001. Contribution of waters of Atlantic and Pacific origin in the Northeast Water Polynya. *Polar Res* **20**(2): 193–200. DOI: https://doi.org/10.1111/j.1751-8369.2001.tb00056.x

Falck, E, Kattner, G and **Budéus, G.** 2005. Disappearance of Pacific Water in the northwestern Fram Strait. *Geophys Res Lett* **32**(L14): 619. DOI: https://doi.org/10.1029/2005GL023400

Fichefet, T and **Maqueda, MAM.** 1997. Sensitivity of a global sea ice model to the treatment of ice thermodynamics and dynamics. *J Geophys Res* **102**: 12609–12646. DOI: https://doi.org/10.1029/97JC00480

Forest, A, Osborne, PD, Curtiss, G and **Lowings, MG.** 2016. Current surges and seabed erosion near the shelf break in the Canadian Beaufort Sea: A response to wind and ice motion stress. *J Mar Sys* **160**: 1–16. DOI: https://doi.org/10.1016/j.jmarsys.2016.03.008

Forest, A, Osborne, PD, Fortier, L, Sampei, M and **Lowings, MG.** 2015. Physical forcings and intense shelf-slope fluxes of particulate matter in the halocline waters of the Canadian Beaufort Sea during winter. *Cont Shelf Res* **101**: 1–21. DOI: https://doi.org/10.1016/j.csr.2015.03.009

Gratton, Y, Ingram, G, Carmack, E, Van Hardengerget, B, Forest, A, Fortier, L, Blondeau, S, Massot, P and **Michaud, L.** (Unpublished). Long-term oceanic observatories (moorings) in the Beaufort Sea during the Canadian Arctic Shelf Exchange Study, 2002–2004. DOI: https://doi.org/10.5884/11653

Hu, X and **Myers, PG.** 2013. A Lagrangian view of Pacific water inflow pathways in the Arctic Ocean during model spin-up. *Ocean Modelling* **71**: 66–80. DOI: https://doi.org/10.1016/j.ocemod.2013.06.007

Hu, X, Sun, J, Chan, TO and **Myers, PG.** 2018. Thermodynamic and dynamic ice thickness changes in the Canadian Arctic Archipelago in NEMO-LIM2 numerical simulations. *Cryosphere Discuss*. DOI: https://doi.org/10.5194/tc-2017-197

Hunke, EC and **Dukowicz, JK.** 1997. An elastic-viscous-plastic model for sea ice dynamics. *J Phys Oceanogr* **27**: 1849–1867. DOI: https://doi.org/10.1175/1520-0485(1997)027<1849:AEVPMF>2.0.CO;2

Jones, EP, Swift, JH, Anderson, JG, Lipizer, M, Civitarese, G, Falkner, KK, Kattner, G and **McLaughlin, FA.** 2003. Tracing Pacific water in the North Atlantic Ocean. *J Geophys Res* **108**(C4): 3116. DOI: https://doi.org/10.1029/2001JC001141

Kalnay, E, Kanamitsu, M, Kistler, R, Collins, W, Deaven, D, Gandin, L, Iredell, M, Saha, S, White, G, Woollen, J, Zhu, Y, Chelliah, M, Ebisuzaki, W, Higgins, W, Janowiak, J, Mo, KC, Ropelewski, C, Wang, J, Leetma, A, Reynolds, R, Jenne, R and **Joseph, D.** 1996. The NCEP/NCAR 40-Year Reanalysis Project. *Bull Amer Meteor Soc* **77**: 437–471. DOI: https://doi.org/10.1175/1520-0477(1996)077<0437:TNYRP>2.0.CO;2

Kirillov, S, Dmitrenko, I, Tremblay, B, Gratton, Y, Barber, D and **Rysgaard, S.** 2016. Upwelling of Atlantic Water along the Canadian Beaufort Sea continental slope: Favorable atmospheric conditions and seasonal and interannual variations. *J Climate* **29**(12): 4509–4523. DOI: https://doi.org/10.1175/JCLI-D-15-0804.1

Kulikov, EA, Carmack, EC and **Macdonald, RW.** 1998. Flow variability at the continental shelf break of the Mackenzie Shelf in the Beaufort Sea. *J Geophys Res* **103**(C6): 12725–12741. DOI: https://doi.org/10.1029/97JC03690

Lin, P, Pickart, RS, Stafford, KN, Moore, GWK, Torres, DJ, Bahr, F and **Hu, J.** 2016. Seasonal variation of the Beaufort shelfbreak jet and its relationship to Arctic cetacean occurrence. *J Geophys Res Oceans* **121**: 8434–8454. DOI: https://doi.org/10.1002/2016JC011890

Madec, G. 2008. NEMO ocean engine. *Note du Pôle de modélisation*, Institut Pierre-Simon Laplace (IPSL), France, 27, ISSN No: 1288-1619.

Martin, T, Steele, M and **Zhang, J.** 2014. Seasonality and long-term trend of Arctic Ocean surface stress in a model. *J Geophys Res Oceans* **119**: 1723–1738. DOI: https://doi.org/10.1002/2013JC009425

Masina, S, Storto, A, Ferry, N, Valdivieso, M, Haines, K, Balmaseda, M, Zuo, H, Drevillon, M and **Parent, L.** 2017. An ensemble of eddy-permitting global ocean reanalyses from the MyOcean project. *Climate Dynamics* **49**: 813–841. DOI: https://doi.org/10.1007/s00382-015-2728-5

Nikolopoulos, A, Pickart, RS, Fratantoni, PS, Shimada, K, Torres, DJ and **Jones, EP.** 2009. The western Arctic boundary current at 152°W: Structure, variability, and transport. *Deep-Sea Res II* **56**: 1164–1181. DOI: https://doi.org/10.1016/j.dsr2.2008.10.014

Nurser, AJG and **Bacon, S.** 2014. The Rossby radius in the Arctic Ocean. *Ocean Sci* **10**: 967–975. DOI: https://doi.org/10.5194/os-10-967-2014

O'Brien, MC, Melling, H, Pedersen, TF and **Macdonald, RW.** 2011. The role of eddies and energetic ocean phenomena in the transport of sediment from shelf to basin in the Arctic. *J Geophys Res* **116**(C08): 001. DOI: https://doi.org/10.1029/2010JC006890

Pickart, RS. 2004. Shelfbreak circulation in the Alaskan Beaufort Sea: Mean structure and variability. *J Geophys Res* **109**(C04): 024. DOI: https://doi.org/10.1029/2003JC001912

Pickart, RS, Moore, GWK, Torres, DJ, Fratantoni, PS, Goldsmith, RA and **Yang, J.** 2009. Upwelling on the continental slope of the Alaskan Beaufort Sea: Storms, ice, and oceanographic response. *J Geophys Res* **114**(C00A1): 3. DOI: https://doi.org/10.1029/2008JC005009

Pickart, RS, Spall, MA and **Mathis, JT.** 2013. Dynamics of upwelling in the Alaskan Beaufort Sea and associated shelf–basin fluxes. *Deep Sea Res I* **76**: 35–51. DOI: https://doi.org/10.1016/j.dsr.2013.01.007

Schulze, LM and **Pickart, RS.** 2012. Seasonal variation of upwelling in the Alaskan Beaufort Sea: Impact of sea ice cover. *J Geophys Res* **117**(C06): 022. DOI: https://doi.org/10.1029/2012JC007985

Smith, GC, Roy, F, Mann, P, Dupont, F, Brasnett, B, Lemieux, J-F, Laroche, S and **Bélair, S.** 2014. A new atmospheric dataset for forcing ice–ocean models: Evaluation of reforecasts using the Canadian global deterministic prediction system. *Q J R Meteorol Soc* **140**: 881–894. DOI: https://doi.org/10.1002/qj.2194

Spall, MA, Pickart, RS, Fratantoni, PS and **Plueddemann, AJ.** 2007. Western Arctic shelfbreak eddies: Formation and transport. *J Phys Oceanogr* **38**: 1644–1668. DOI: https://doi.org/10.1175/2007JPO3829.1

Spreen, G, Kaleschke, L and **Heygster, G.** 2008. Sea ice remote sensing using AMSR-E 89 GHz channels. *J Geophys Res* **113**(C02): S03. DOI: https://doi.org/10.1029/2005JC003384

Steele, M, Morison, J, Ermold, W, Rigor, I, Ortmeyer, M and **Shimada, K.** 2004. Circulation of summer Pacific halocline water in the Arctic Ocean. *J Geophys Res* **109**(C02): 027. DOI: https://doi.org/10.1029/2003JC002009

Timmermans, M-L, Proshutinsky, A, Golubeva, E, Jackson, JM, Krishfield, R, McCall, M, Platov, G, Toole, J, Williams, W, Kikuchi, T and **Nishino, S.** 2014. Mechanisms of Pacific Summer Water variability in the Arctic's Central Canada Basin. *J Geophys Res Oceans* **119**: 7523–7548. DOI: https://doi.org/10.1002/2014JC010273

von Appen, W-J and **Pickart, RS.** 2012. Two configurations of the Western Arctic shelfbreak current in summer. *J Phys Oceanogr* **42**: 329–351. DOI: https://doi.org/10.1175/JPO-D-11-026.1

Watanabe, J. 2013. Linkages among halocline variability, shelf-basin interaction, and wind regimes in the Beaufort Sea demonstrated in pan-Arctic Ocean modeling framework. *Ocean Modelling* **71**: 43–53. DOI: https://doi.org/10.1016/j.ocemod.2012.12.010

Weingartner, T, Cavalieri, D, Aagaard, K and **Sasaki, Y.** 1998. Circulation, dense water formation, and outflow on the northeast Chukchi shelf. *J Geophys Res* **103**(C4): 7647–7661. DOI: https://doi.org/10.1029/98JC00374

Williams, WJ, Carmack, EC, Shimada, K, Melling, H, Aagaard, K, Macdonald, RW and **Ingram, RG.** 2006. Joint effects of wind and ice motion in forcing upwelling in Mackenzie Trough, Beaufort Sea. *Continental Shelf Res* **26**: 2352–2366. DOI: https://doi.org/10.1016/j.csr.2006.06.012

Winsor, P and **Chapman, DC.** 2004. Pathways of Pacific water across the Chukchi Sea: A numerical model study. *J Geophys Res* **109**(C03): 002. DOI: https://doi.org/10.1029/2003JC001962

Yang, J. 2009. Seasonal and interannual variability of downwelling in the Beaufort Sea. *J Geophys Res* **114**(C00A1): 4. DOI: https://doi.org/10.1029/2008JC005084

How to cite this article: Dmitrenko, IA, Kirillov, SA, Myers, PG, Forest, A, Tremblay, B, Lukovich, JV, Gratton, Y, Rysgaard, S and Barber, DG. 2018. Wind-forced depth-dependent currents over the eastern Beaufort Sea continental slope: Implications for Pacific water transport. *Elem Sci Anth,* 6: 66. DOI: https://doi.org/10.1525/elementa.321

Domain Editor-in-Chief: Jody W. Deming, Ph.D., Department of Biological Oceanography, University of Washington, US

Associate Editor: Mary-Louise Timmermans, Yale University, US

Knowledge Domain: Ocean Science

Submitted: 25 May 2018 **Accepted:** 26 September 2018 **Published:** 23 October 2018

ELEMENTA Science of the Anthropocene

Elem Sci Anth is a peer-reviewed open access journal published by University of California Press.

OPEN ACCESS